JOURNAL OF VIROLOGY, Jan. 2006, p. 785–793 Vol. 80, No. 2
0022-538X/06/$08.00+0 doi:10.1128/JVI.80.2.785–793.2006

7a Protein of Severe Acute Respiratory Syndrome Coronavirus Inhibits Cellular Protein Synthesis and Activates p38 Mitogen-Activated Protein Kinase

Sarah A. Kopecky-Bromberg, Luis Martinez-Sobrido, and Peter Palese*

Department of Microbiology, Mount Sinai School of Medicine, New York, New York 10029-6574

Received 20 July 2005/Accepted 16 October 2005

It was recently shown that the 7a protein of severe acute respiratory syndrome coronavirus induces biochemical changes associated with apoptosis. In this study, the mechanism by which the 7a protein induces apoptosis was examined. The 7a protein was tested for the ability to inhibit cellular gene expression because several proapoptotic viral proteins with this function have previously been identified. 7a protein inhibited expression of luciferase from an mRNA construct that specifically measures translation, whereas inhibitors of transcription and nucleocytoplasmic transport did not. The inhibition of translation and other cellular processes of gene expression have been associated with the induction of a stress response in cells. Western blot analysis using phosphospecific antibodies indicated that 7a protein activated p38 mitogen-activated protein kinase (MAPK), but not c-Jun N-terminal protein kinase/stress-activated protein kinase. Taken together, these data indicate that the induction of apoptosis by the 7a protein may be related to its ability to inhibit cellular translation and activate p38 MAPK.

Severe acute respiratory syndrome coronavirus (SARS-CoV) has been identified as an enveloped, positive-sense RNA virus containing a large genome that encodes proteins expressed from full-length and subgenomic mRNAs. The genomic organization of SARS-CoV consists of a large replicase gene that is predicted to encode two polyproteins that undergo cotranslational proteolytic processing. The replicase gene is followed by several genes encoding structural proteins, as well as several predicted nonstructural proteins that are not well characterized and are not encoded by other coronaviruses (21, 28). It is possible that one or more of these proteins may contribute to the high pathogenicity caused by SARS-CoV.

SARS-CoV spread worldwide in 2003, infecting thousands of people and killing hundreds. While it has been demonstrated that death was caused by respiratory illness, the molecular mechanisms of the viral pathogenesis have not been precisely determined. Patients infected with SARS-CoV develop severe pneumonia-like symptoms, but the virus can be found in several other organs, such as the kidney and the liver (4). The immune systems of SARS patients are also affected by the disease. There is a decrease in $CD4^+$ and $CD8^+$ T cells that begins early in the disease and persists for several weeks (37). The extent of the lymphocyte depletion varies among individuals, and a dramatic reduction in the levels of lymphocytes appears to correlate with severe disease symptoms (17, 18). As high amounts of virus have been detected in lymphocytes taken from SARS patients (35), it is possible that the lymphocytes are depleted as a direct result of virus-induced apoptosis. High titers of virus are also found in the lungs, suggesting that virus-induced apoptosis may also contribute to lung pathology. SARS-CoV was reported to induce apoptosis in tissue culture cells, supporting the hypothesis that virus-induced apoptosis may have a role in disease progression (38).

Recently, the SARS-CoV 7a protein (also referred to as open reading frame [ORF] 8, X4, and U122) was demonstrated to cause biochemical changes associated with apoptosis in transfected cells (32). The 7a protein has been shown to be expressed in SARS-CoV-infected tissue culture cells and in lung tissue obtained from SARS-CoV patients (3, 6). It has also been revealed that 7a protein coimmunoprecipitates with another SARS-CoV protein, 3a protein (also known as ORF 3, ORF 3a, X1, and U274), suggesting that the 7a protein and the 3a protein may interact in virus-infected cells (33). Comparison of the 7a amino acid sequence with those of other known human and viral proteins yielded no homology. The 7a protein is 122 amino acids long, has a signal sequence, has a predicted transmembrane helix from residues 95 to 117, and is likely a membrane protein (6). The function of 7a protein and its role in the pathogenesis caused by SARS-CoV are not well characterized. Part of the 7a protein (amino acids 16 to 80) has been crystallized, and the structure was resolved (23). The luminal domain of 7a protein adopts a compact immunoglobulin-like β sandwich fold. This fold is present in many different proteins, including cell surface receptors, transcription factors, and enzymes, and is not indicative of the function of 7a protein.

In the present study, it was confirmed that 7a protein induces apoptosis by analysis of both morphological and biochemical changes associated with apoptosis. In addition, it was determined that 7a protein inhibits cellular gene expression. Further analysis revealed that 7a protein inhibits cellular gene expression at the level of translation. There are discrepancies in the literature as to the localization of 7a protein. The data presented here indicate that 7a protein is, in fact, localized to the Golgi. It was also determined that expression of the 7a

* Corresponding author. Mailing address: Department of Microbiology, Mount Sinai School of Medicine, New York, NY 10029-6574. Phone: (212) 241-7318. Fax: (212) 534-1684. E-mail: peter.palese@mssm.edu.

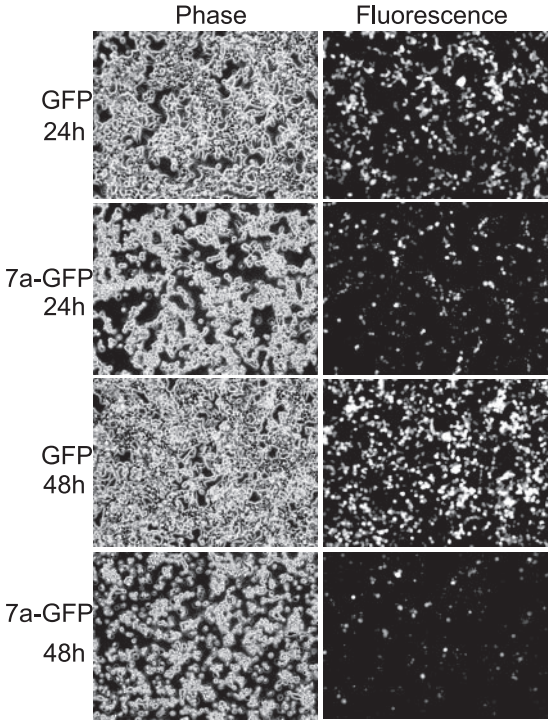

FIG. 1. Expression of the fusion protein 7a-GFP causes morphological changes associated with apoptosis. 293T cells were transfected with either GFP plasmid or 7a-GFP plasmid for 24 or 48 h, as indicated in the figure. Phase-contrast and fluorescence images were obtained by using an inverted Zeiss Axiovert 200 microscope. Images are representative of three independent experiments.

protein activates p38 mitogen-activated protein kinase (MAPK), which is also activated in SARS-CoV-infected cells (22).

MATERIALS AND METHODS

Cells and plasmids. 293T, A549, and HeLa cells were cultured in Dulbecco's modified Eagle medium containing 10% fetal bovine serum. The enhanced green fluorescent protein (GFP) ORF from the plasmid pEGFP-c1 (Clontech) was cloned into the pCAGGS plasmid. The 7a protein was amplified by reverse transcription-PCR from lysates of cells infected with the Urbani strain of SARS-CoV and cloned into GFP or hemagglutinin (HA) pCAGGS. The GFP and HA tags are on the C-terminal end of 7a protein. pGL3 control luciferase-expressing plasmid was purchased from Promega.

In vitro-transcribed mRNA and transfections. To synthesisze the luciferase mRNA, the luciferase gene was cloned from the pGL3 plasmid into the pGEM-4Z plasmid (Promega) by using the XbaI and HindIII restriction sites. Luciferase pGEM-4Z was linearized with BamHI. In vitro-transcribed mRNA was synthesized with the message machine T7 Ultra kit (Ambion). The resulting mRNAs contained 5′ caps and 3′ poly(A) sequences. For transfections, cells were seeded onto 24-well plates, 6-well plates, or 100-mm plates; the monolayers were transfected the following day with 200 ng, 1 μg, or 5 μg of plasmid or mRNA and 1 μl, 5 μl, or 40 μl of Lipofectamine 2000 reagent (Invitrogen) and brought to a total volume of 300 μl, 1.2 ml, or 8 ml with Optimem (Invitrogen), respectively.

Microscopy. 293T cells were seeded in six-well dishes and transfected with GFP pCAGGS or 7a-GFP pCAGGS. At the indicated times, the cells were analyzed using an inverted Zeiss Axiovert 200 microscope (Fig. 1). 293T cells were seeded in 24-well dishes and transfected with the indicated amounts of 7a-GFP pCAGGS (Fig. 2). Cells were analyzed by microscopy at 24 h posttransfection. HeLa cells were seeded in 24-well dishes on coverslips (see Fig. 6). At 8 h posttransfection, cells were fixed with 5% formaldehyde and permeabilized with 1% Triton X-100. Cells were incubated with blocking buffer (phosphate-buffered

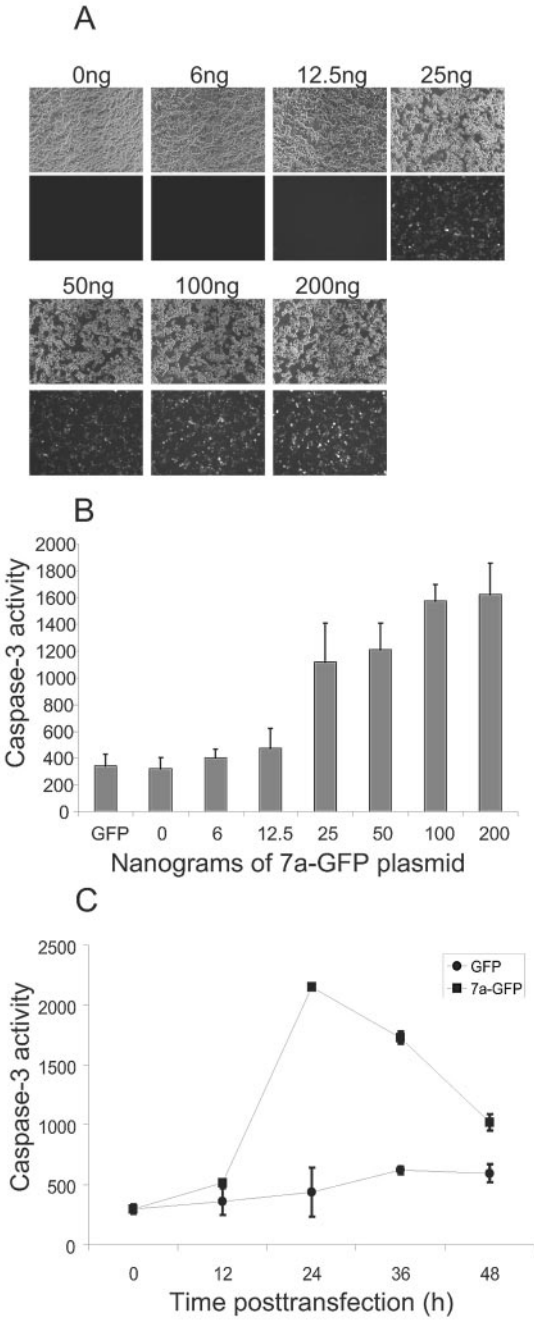

FIG. 2. 7a-GFP activates caspase-3. (A) A total of 2×10^5 293T cells were transfected with GFP plasmid or the indicated amounts of 7a-GFP plasmid. The total amount of DNA transfected was held constant at 200 ng in all samples by the addition of empty vector plasmid. Cells were analyzed by microscopy at 24 h posttransfection. (B) A total of 2×10^5 293T cells were transfected with GFP plasmid or the indicated amounts of 7a-GFP plasmid. Cells were harvested at 24 h, and capsase-3 activity was measured using a DEVD-AFC fluorogenic substrate. The amount of caspase-3 activated is expressed in arbitrary fluorescence units. The data represent the averages ± the standard deviation of three experiments. (C) A total of 2×10^5 293T cells were transfected with either 200 ng GFP plasmid or 7a-GFP plasmid for the times indicated. Cells were analyzed for caspase-3 activity as described in the legend to panel A. The data represent the averages ± the standard deviation of three experiments.

saline [PBS], 0.05% Tween, 0.5% bovine serum albumin, 0.8% glycine) for 5 min and then incubated with primary antibody at a dilution of 1:500 for 1 h at room temperature. Primary antibodies used were mouse anti-cytochrome *c* (Pharmingen), rabbit anti-protein disulfide isomerase (PDI; a kind gift from Domenico Tortorella), mouse anti-HA tag (Sigma), and mouse anti-7a (a kind gift from Ralph Baric). Cells were washed three times with blocking buffer and then incubated with donkey anti-mouse Alexa Fluor 488, donkey anti-rabbit 594, donkey anti-mouse 596, or BODIPY TR (all from Molecular Probes) at a dilution of 1:500 for 1 h. Cells were incubated with 4′,6-diamidino-2-phenylindole-dihydrochloride (DAPI; Molecular Probes) for 5 min. Cells were washed three times, and coverslips were mounted on slides with Aqua Polymount (Polysciences). Slides were analyzed by confocal microscopy with Zeiss LSM 510 Meta. 293T cells were seeded in 24-well dishes, transfected with GFP or 7a-GFP plasmid in the absence or presence of SB203580 (Sigma), stained with DAPI, and analyzed at 24 h (see Fig. 8).

Caspase-3 activity assay. 293T cells were seeded in 24-well dishes and transfected with the indicated amounts of GFP plasmid or 7a-GFP plasmid for the indicated times. The total amount of DNA transfected was held constant at 200 ng in all samples with the addition of empty vector plasmid. Cells were lysed and analyzed for caspase-3 activity according to the manufacturer's protocol (R&D Systems). Fluorescence was measured in a Versafluor fluorometer (Bio-Rad).

Luciferase assay. 293T cells were seeded in 24-well dishes and transfected with either pGL3 or luciferase mRNA and GFP plasmid or 7a-GFP plasmid for the indicated times. Some samples were also treated with 5-μg/ml actinomycin D (Act D), 50-μg/ml cycloheximide (Cyclo), or 5-ng/ml leptomycin B (Lep B) at the time of transfection (all from Sigma) (see Fig. 4). Cells were harvested, lysed, and analyzed for luciferase according to the manufacturer's protocol (Promega). Luminescence was measured in a Mini Lumat luminometer (Berthold).

Cellular protein synthesis assay. 293T cells were seeded in six-well dishes and transfected with GFP plasmid or 7a-GFP plasmid. At 4, 8, and 12 h postinfection, cells were incubated in Dulbecco's modified Eagle medium without methionine or cysteine for 10 min. Cells were then labeled with [^{35}S]methionine at a concentration of 100 μCi per ml for 10 min. Cells were washed and solubilized with buffer (PBS, 1% NP-40, 0.5% deoxycholate, 0.1% sodium dodecyl sulfate [SDS], 1 mM EDTA) supplemented with protease inhibitor cocktail (Complete; Roche). Lysates were spun down, and protein content was determined by Bradford assay (Bio-Rad) according to the manufacturer's protocol. Aliquots of lysates representing equal amounts of protein were analyzed by SDS-polyacrylamide gel electrophoresis (SDS-PAGE) using a 10% acrylamide gel. The gels were fixed with 25% 2-propanol and 10% glacial acetic acid, dried, and exposed to film.

Western blot analysis. 293T cells were seeded in 100-mm dishes and transfected with GFP plasmid or 7a-GFP plasmid or treated with 1-μg/ml anisomycin for the indicated times (see Fig. 7). Cells were harvested, lysed in buffer (PBS, 1% NP-40, 0.5% deoxycholate, 0.1% SDS, and 1 mM EDTA) supplemented with protease inhibitor cocktail (Complete; Roche), and spun down to remove nuclei. The protein content was determined by Bradford assay (Bio-Rad). Aliquots of lysates representing equal amounts of protein were analyzed by SDS-PAGE. The proteins were transferred to a nitrocellulose membrane and probed with antibodies against phospho-c-Jun N-terminal protein kinase (phospho-JNK)/stress-activated protein kinase, total JNK/stress-activated protein kinase, phospho-p38 MAPK, and total p38 MAPK (Cell Signaling Technology). After incubation with an anti-rabbit peroxidase-labeled secondary antibody (Amersham), blots were analyzed by chemiluminescence (Perkin-Elmer). Cells were transfected with 7a-GFP plasmid in the absence or presence of Z-VAD (R&D systems) or SB203580 p38 MAPK inhibitor (see Fig. 8). An immunoblot for phospho-p38 was performed, and p38 activity was measured using a p38 activity kit (Sigma) according to the protocol (see Fig. 8).

RESULTS

Expression of SARS-CoV 7a protein induces apoptotic changes. While 7a protein has been reported to induce biochemical changes associated with apoptosis, it has not been determined whether 7a protein causes apoptotic morphological changes. To further examine whether SARS-CoV 7a protein induces apoptosis, 293T cells were transfected with a plasmid expressing the 7a-GFP fusion construct or with a plasmid expressing GFP as a negative control. 7a protein was fused with GFP so cells expressing 7a protein could be easily distinguished from nontransfected cells. It has been reported previously that the level of expression of 7a protein in transfected cells is similar to the level of 7a protein in SARS-CoV-infected cells (23). Cells were analyzed for the morphological changes associated with apoptosis using phase-contrast and fluorescence microscopy at 24 and 48 h posttransfection (Fig. 1). Cells expressing GFP remained elongated, similar to nontransfected cells (Fig. 1 and data not shown). Cells expressing 7a-GFP for 24 h displayed cell rounding, cell shrinkage, apoptotic changes, and cells expressing 7a-GFP for 48 h displayed cell blistering, a morphological change that occurs prior to membrane perforation. These data indicate that 7a protein causes cells to undergo apoptosis.

To further corroborate the induction of apoptosis by 7a protein, GFP or different amounts of 7a-GFP were transfected into 293T cells (Fig. 2A). The induction of cytopathic effects caused by 7a protein correlated with expression levels of 7a protein at 24 h posttransfection. These results were confirmed by analyzing the biochemical changes associated with apoptosis. Cells were harvested at 24 h posttransfection and analyzed for caspase-3, a major enzyme activated during the induction of apoptosis (Fig. 2B). As little as 25 ng of 7a-GFP per well of a 24-well dish was sufficient to activate caspase-3, while maximal caspase-3 activation was observed when 100 ng per well was used. Figure 2C shows a time course of caspase-3 activation after expression of 7a-GFP. Cells were harvested at 0, 12, 24, 36, and 48 h posttransfection. At 12 h posttransfection, there was only little caspase-3 activation above the negative control, but by 24 h, there were significant levels of capsase-3 present, indicating that apoptotic effectors were activated during this time. There was a decrease of caspase-3 activation by 7a-GPF at 36 and 48 h posttransfection. This is most likely due to the fact that as the cells die, the membrane perforates, and the caspase-3 in the cytoplasm leaks out of the cells (12, 13). These results were confirmed by transfecting a plasmid encoding an HA-tagged 7a protein (data not shown).

The 7a protein inhibits cellular gene expression. While it has been demonstrated that 7a protein induces apoptosis (32), the precise mechanism of apoptosis has not been clear. Many RNA viruses, including other positive-sense RNA viruses such as poliovirus, encode proteins that induce apoptosis. Several of these proteins induce apoptosis as a consequence of an inhibition of cellular gene expression. The inhibition of cellular gene expression results in blocking the synthesis of antiviral genes, such as interferon. Thus, these viral proteins prevent an antiviral state by inhibiting cellular gene expression but also induce apoptosis, since cellular gene expression is necessary for survival. To determine whether 7a protein inhibits cellular gene expression, cells were cotransfected with a plasmid expressing GFP or 7a-GFP and a plasmid expressing firefly luciferase from a simian virus 40 promoter, a typical polymerase II promoter. Cells were harvested at various times posttransfection, lysed, and analyzed for cellular gene expression by measuring firefly luciferase activity (Fig. 3). Cells cotransfected with plasmids encoding GFP and luciferase displayed an increasing amount of luciferase over the 12-h time course, as would be expected of normally functioning cells. Cells cotransfected with plasmids encoding 7a-GFP and luciferase showed a much smaller increase in cellular gene expression over the time

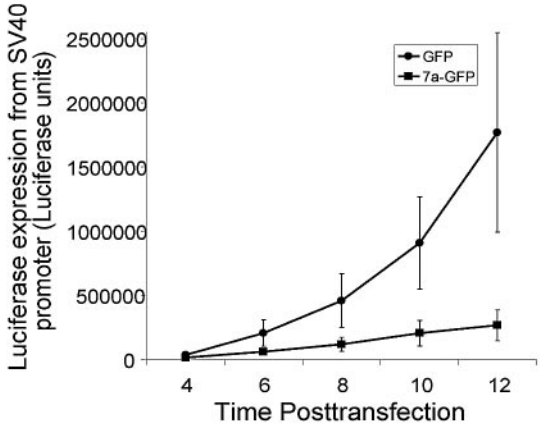

FIG. 3. 7a-GFP inhibits cellular gene expression. A total of 2×10^5 293T cells were transfected with the 200 ng luciferase-expressing plasmid pGL3 and either 200 ng GFP plasmid or 200 ng 7a-GFP plasmid. Cells were harvested at the indicated times and analyzed for luciferase activity by using a luciferase substrate. The amount of luciferase present is expressed in arbitrary luminescence units. The data represent the averages ± the standard deviation of three experiments.

course. This indicates that cellular gene expression is inhibited in cells expressing 7a-GFP.

The 7a protein inhibits protein translation. Cellular gene expression can be inhibited on several levels, including transcription, translation, and nucleocytoplasmic transport of RNAs and proteins. To identify the cellular process that is inhibited by 7a protein, the effect of 7a protein was compared to that of an inhibitor of transcription, Act D; an inhibitor of translation, Cyclo; and an inhibitor of nucleocytoplasmic transport, Lep B. Host gene expression was measured by cotransfection of a luciferase plasmid and analysis of luciferase activity as shown in Fig. 3. Cellular protein synthesis was measured by cotransfection of in vitro-transcribed luciferase mRNA and analysis of luciferase activity. By using luciferase mRNA, translation can be measured without the requirement for transcription and nucleocytoplasmic transport. Cells were cotransfected either with luciferase plasmid (Fig. 4A) or luciferase mRNA (Fig. 4B) and with 7a-GFP plasmid or with GFP plasmid and treated with the inhibitors. As in the data shown in Fig. 3, 7a-GFP dramatically inhibited cellular gene expression by nearly 90% (Fig. 4A). The synthetic inhibitors of cellular processes were also effective at inhibiting cellular gene expression. The results of the cellular translation analysis differ markedly. Cyclo was able to effectively inhibit cellular translation as predicted. However, Act D and Lep B did not inhibit cellular translation and actually caused an increase in cellular translation over the GFP samples. This is likely due to the fact that the absence of new transcripts caused the mRNAs present to be translated at a higher rate, since there was reduced competition for translation machinery. 7a-GFP inhibited cellular translation by nearly 50%, suggesting that the mechanism of inhibition of cellular gene expression by 7a protein is translation. 7a protein also inhibited translation in A549 cells (data not shown). There was less apparent inhibition of translation by 7a protein (Fig. 4A) than inhibition of total cellular gene expression (Fig. 4B) (50% to 90%). This is likely because the luciferase mRNA is expressed rapidly after transfection, while

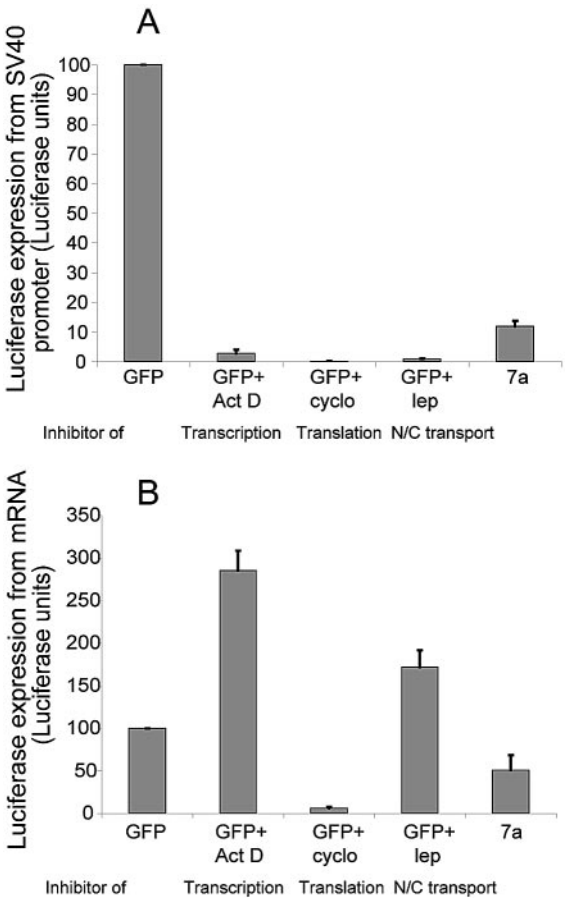

FIG. 4. 7a-GFP inhibits expression of luciferase from an mRNA construct. A total of 2×10^5 293T cells were transfected with either 200 ng pGL3 (A) or 1 ng luciferase mRNA (B) and 200 ng GFP plasmid or 200 ng 7a-GFP plasmid, as indicated. Some samples were also treated with Act D, Cyclo, or Lep B at the time of transfection. Cells were harvested at 12 h posttransfection and analyzed for luciferase as described in the legend to Fig. 3. The data represent the averages ± the standard deviation of three experiments.

it takes several hours for the 7a-GFP to be expressed from a plasmid. Thus, luciferase is probably expressed before the 7a protein inhibition is apparent. Indeed, it takes 6 h for 7a-GFP to be visible in a fluorescence microscope after transfection (data not shown). There was greater inhibition of translation by 7a protein (74.8% ± 13.7%) when cells were transfected with 7a protein for 12 h and then transfected with luciferase mRNA for an additional 12 h.

To confirm the inhibition of protein synthesis by 7a protein, 293T cells were transfected with a GFP plasmid or a plasmid expressing 7a-GFP and pulsed with [^{35}S]methionine at 4, 8, or 12 h posttransfection for 10 min. Cells were washed, harvested, and lysed, and lysates were analyzed by SDS-PAGE. The gel was exposed to film, and a representative experiment is shown in Fig. 5. By this technique, only proteins synthesized during a 10-min period at each time point were analyzed. There was little difference in translation levels of cells expressing GFP and 7a-GFP at 4 h posttransfection. Cells transfected with 7a-GFP displayed reduced protein synthesis at 8 h and even greater inhibition of protein synthesis at 12 h than cells trans-

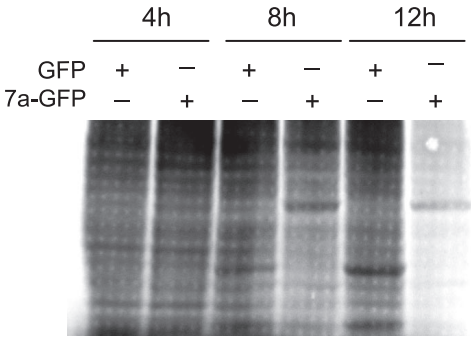

FIG. 5. 7a-GFP inhibits cellular protein synthesis. A total of 10^6 293T cells were transfected with either 1 μg GFP plasmid or 1 μg of 7a-GFP plasmid. At 4, 8, and 12 h posttransfection, cells were labeled with [^{35}S]methionine for 10 min, and lysates were analyzed by SDS-PAGE. Dried gels were exposed to film. A representative image from three independent experiments is shown.

fected with GFP. These results were confirmed by transfecting a plasmid encoding an HA-tagged 7a protein (data not shown). Thus, the data shown in Fig. 4 and 5 indicate that 7a protein inhibits protein synthesis.

The 7a protein localizes to the Golgi apparatus. The inhibition of cellular protein synthesis by 7a protein was unexpected, since 7a protein was not predicted to be in the cytosol where the translation machinery is located. There are discrepancies in the literature as to the cellular localization of the 7a protein. The 7a protein contains a predicted signal sequence and is thought to be synthesized in the endoplasmic reticulum (ER). A report indicates that it is retained there (6), but other reports suggest that it is transported to the Golgi (23). To determine the localization of 7a protein, GFP and 7a-GFP were transfected into HeLa cells and stained with markers for intracellular organelles. 293T cells were not used for these experiments because they are quite small and the organelles are difficult to distinguish in the confocal microscope. In these experiments, the Golgi was visualized using the BODIPY TR Golgi marker, the ER was visualized with an antibody to PDI, the mitochondria were visualized with an antibody to cytochrome *c*, and the DNA was visualized with DAPI. Representative images are shown in Fig. 6. Cells expressing GFP (Fig. 6A) displayed GFP fluorescence throughout the nucleus and cytoplasm, but GFP did not localize in intracellular compartments, as seen by the absence of yellow overlay in the cells labeled with the Golgi, ER, and mitochondrial markers. In contrast, 7a-GFP strongly colocalized with the Golgi marker (Fig. 6B). These results were confirmed by using another Golgi marker, wheat germ agglutinin (data not shown). 7a-GFP did

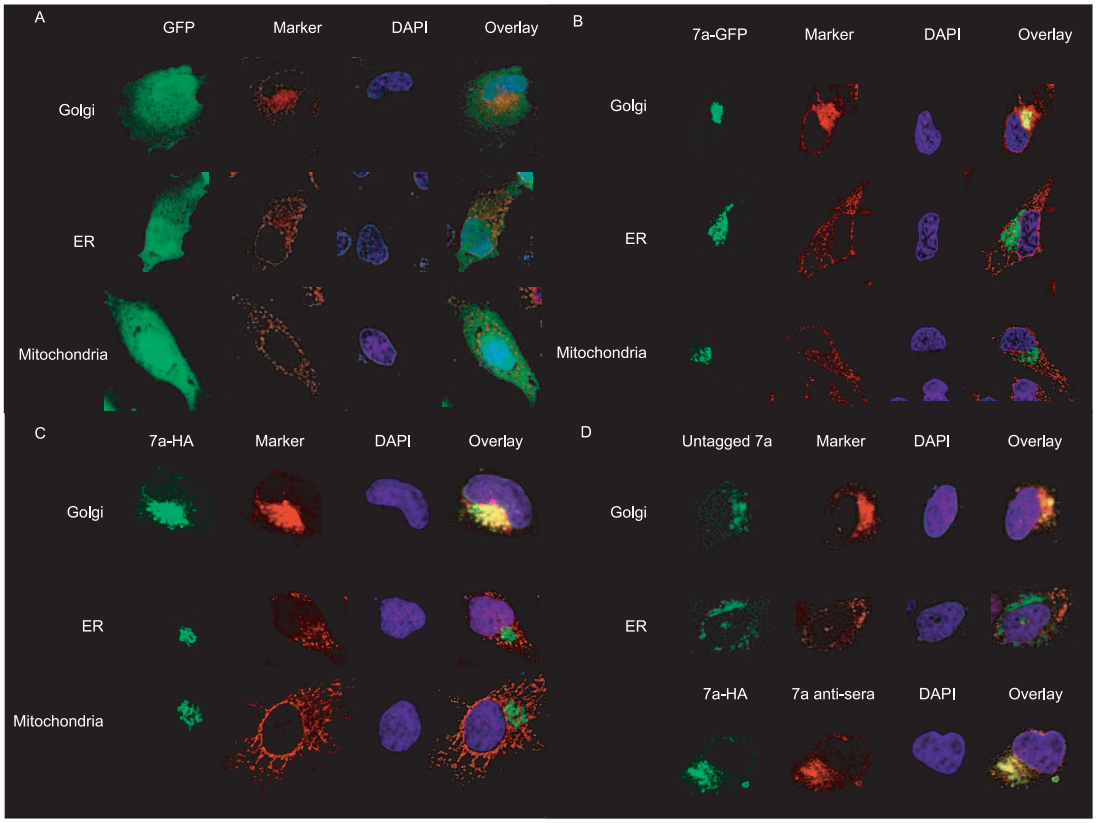

FIG. 6. 7a-GFP is localized to the Golgi. A total of 2×10^5 HeLa cells were transfected with either GFP plasmid (A), 7a-GFP plasmid (B), 7a-HA plasmid (C and D, bottom row), or untagged 7a plasmid (D, top two rows) for 8 h. Cells were fixed, permeabilized, and stained for either the Golgi with BODIPY TR, the ER with an antibody to PDI, the mitochondria with an antibody to cytochrome *c*, or chromatin with a DAPI stain. Untagged 7a protein was visualized with 7a antisera provided by Ralph Baric. Green coloring represents GFP (A) 7a-GFP (B), 7a-HA (C), and untagged 7a (D, top two rows) or 7a-HA (D, bottom row). Red coloring represents the indicated organelle, and blue coloring represents the chromatin. Images are representative of three independent experiments.

not appear to localize to the ER, mitochondria, or nucleus. Thus, 7a-GFP is likely synthesized in the ER and then quickly localizes to the Golgi. In addition, a 7a construct was tested that contained an HA tag (Fig. 6C). The 7a-HA construct also localized to the Golgi but did not localize to the ER, mitochondria, or nucleus. To rule out the possibility that the tags altered localization of 7a protein, an untagged 7a protein was also tested (Fig. 6D, top two rows). The untagged 7a protein was visualized with 7a antisera, which colocalized well with the tagged forms of 7a protein (7a-HA) (Fig. 6D, bottom row). The untagged 7a protein also localized to the Golgi. Our results agreed with those of Nelson et al., where it was described that 7a localizes to the Golgi apparatus in SARS-CoV-infected cells (23).

p38 MAPK, but not JNK, is activated by expression of 7a protein. Very few Golgi proteins have been demonstrated to induce apoptosis, and a link between protein synthesis and the Golgi has not been clearly described. It is likely that 7a protein does not directly interact with translation factors or caspases but rather interacts with an upstream protein(s) that activates downstream enzymes, resulting in the observed cellular consequences. One possibility is that the induction of apoptosis by 7a protein is a result of a stress response and that inhibition of translation is a cellular stress. A stress response often causes the activation of MAPK pathways. Two MAPK pathways associated with a stress response and apoptosis are p38 MAPK and JNK. JNK has been associated with a stress response originating in the ER, while p38 MAPK has not (16, 22). p38 and JNK can be transiently activated by various stimuli, including inhibition of host gene expression; such an insult can lead to apoptosis (10, 11). Recently, it has been determined that p38 MAPK is activated during infection with SARS-CoV (22).

To determine whether p38 or JNK was activated by 7a protein, cells were transfected with GFP for 12 h or with 7a-GFP for 6, 12, or 24 h. Cells were harvested, lysed, and analyzed by SDS-PAGE. Western blots were performed using antibodies against the activated, phosphorylated forms of p38 and JNK and antibodies recognizing the total amount of these proteins. Western blots from representative experiments are shown in Fig. 7. JNK was not activated by 7a-GFP, whereas JNK was activated by the positive control, anisomycin. While there is a low level of activated p38 normally found in 293T cells, expression of 7a-protein stimulated larger amounts of activated p38 during the 24-h time course. To determine whether activation of caspase pathways was required for the activation of p38, cells were transfected with 7a-GFP in the presence of a pan-caspase inhibitor, Z-VAD (Fig. 8A). The caspase inhibitor did not prevent p38 activation induced by 7a protein in either A549 cells or 293T cells. These data indicate that the caspases are not required for the activation of p38 MAPK by 7a protein.

To determine whether apoptosis induced by 7a protein requires activation of p38 MAPK, the p38 inhibitor SB203580 was analyzed. SB203580 prevented activity of p38, as measured by immunoprecipitation with p38 MAPK and analysis for the active form of activating transcription factor 2, a substrate of active p38 (Fig. 8B). SB203580 did not prevent apoptosis induced by 7a protein (Fig. 8C). Cell rounding and chromatin condensation visualized with DAPI were present in cells expressing 7a protein in the presence of SB203580. SB203580 also did not prevent 7a protein-induced inhibition of translation (data not shown). These data indicate that 7a protein likely activates proapoptotic pathways in addition to the p38 pathway.

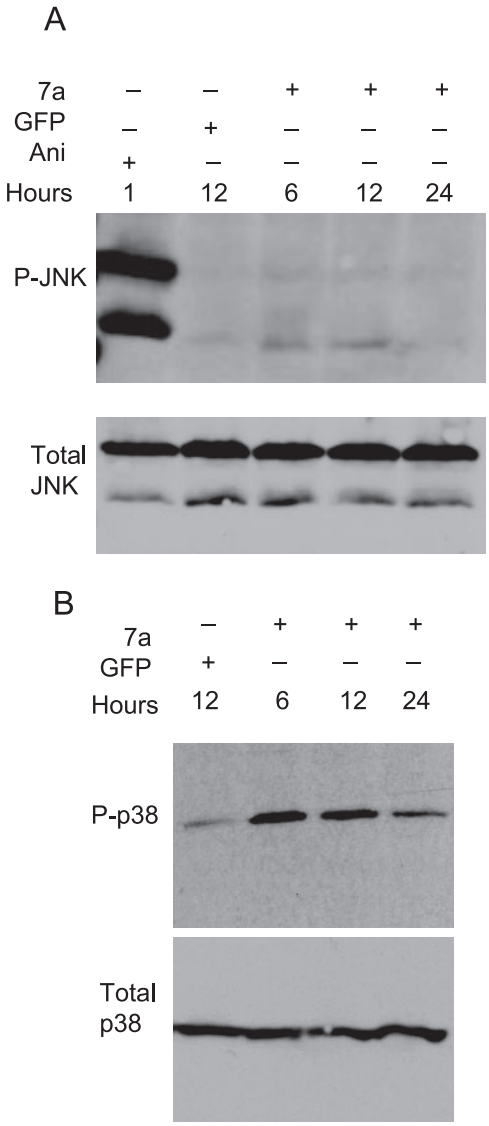

FIG. 7. p38 MAPK is activated by expression of 7a-GFP. A total of 10^6 293T cells were either transfected with GFP or 7a-GFP plasmids or treated with anisomycin for the times indicated. Cells were harvested, lysed, and analyzed for protein content by a Bradford assay. Lysates were divided into aliquots representing equal amounts of protein and analyzed by SDS-PAGE. Western blots were performed using antibodies recognizing phospho-JNK, total JNK, phospho-p38 MAPK, and total p38 MAPK. Images are representative of three independent experiments.

DISCUSSION

An important goal is to determine the reason for the high pathogenicity of SARS-CoV in humans. This question can be addressed by determining the mechanism by which SARS-CoV is targeted to specific organs. The viral receptor for SARS-CoV was found to be angiotensin-converting enzyme 2 (ACE2), and ACE2 is believed to function in cardiac regula-

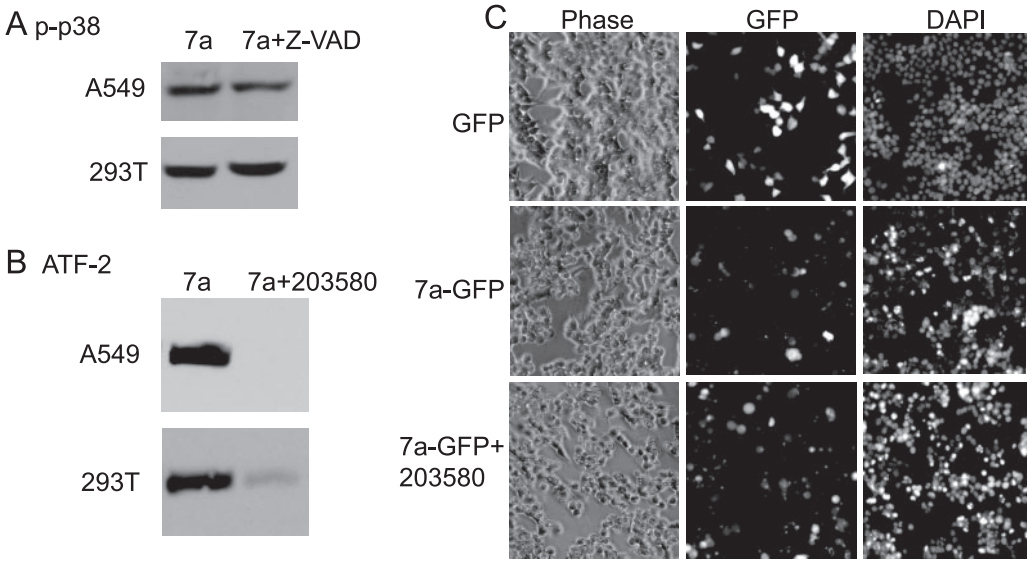

FIG. 8. Induction of apoptosis by 7a protein in the presence of a p38 MAPK inhibitor. (A) A total of 10^6 A549 cells or 293T cells were transfected with 7a-GFP plasmid in the absence or presence of general caspase inhibitor Z-VAD (200 μM). Cells were harvested at 12 h posttransfection and analyzed for phospho-p38 MAPK as described in the legend to Fig. 7. (B) A total of 3×10^6 A549 cells or 293T cells were transfected with 7a-GFP plasmid in the absence or presence of p38 MAPK inhibitor SB203580. Cells were analyzed for p38 activity with a p38 MAPK activity assay kit. The assay is based on immunoprecipitation of the active form of p38 MAPK and detection of its phosphorylation activity on activating transcription factor 2, a p38 MAPK substrate by immunoblotting. (C) A total of 2×10^5 293T cells were transfected with GFP plasmid or 7a-GFP plasmid in the absence or presence of 25 μM SB203580 p38 MAPK inhibitor. Cells were analyzed by microscopy at 24 h posttransfection.

tion (19). Since ACE2 is highly expressed in heart, testes, and kidney but not in other tissues, viral tropism is likely determined by a mechanism other than a viral receptor; this mechanism is currently under investigation (5, 34).

The mechanism by which infection with some viruses causes severe symptoms has been studied extensively. For several viruses, it has been shown that virus-induced apoptosis contributes to pathology and disease symptoms. It has been suggested that apoptosis contributes to the severe disease caused by infection with SARS-CoV (24). The induction of apoptosis by SARS-CoV in tissue culture cells and the induction of biochemical changes associated with apoptosis by SARS-CoV 7a protein has been previously reported (32, 38). It has also been reported that both SARS-CoV and another coronavirus, mouse hepatitis virus, activate p38 MAPK (1, 22). However, it was unknown whether 7a protein had any other effects on cells. In the manuscript, it was shown that 7a protein inhibits cellular protein synthesis and activates the p38 MAPK pathway. SARS coronavirus may encode other proteins that activate p38 MAPK. As it appears that activation of p38 MAPK contributes to cytopathogenesis of SARS-CoV, it is likely that any contribution to p38 MAPK activation is significant (22).

The results presented here are especially interesting, since 7a protein is present in the Golgi. Nelson et al. demonstrated that the cytoplasmic tail of 7a protein is responsible for targeting the protein to the Golgi (23). The role of the Golgi in the induction of apoptosis has not been well characterized. It is known that the Golgi is fragmented during apoptosis. Several Golgi proteins have been identified as targets for cleavage by caspases. One of these proteins is Golgin-160, a Golgi protein that is believed to function in Golgi structure and membrane traffic (8, 20). Another caspase target, p115, has roles in Golgi structure and also binds two other Golgi proteins, GM130 and giantin (31). This complex is believed to promote the tethering of transport vesicles. GRASP65 is also cleaved by caspases, is important for the reconstitution of the Golgi after mitosis, and may also have roles in binding p115 to GM130 (2, 31). Thus, cleavage of these proteins promotes the disassembly of the Golgi and the disruption of membrane traffic. The disassembly of the Golgi appears to be necessary for the packaging of the organelle in apoptotic membrane blebs. The disassembly of the Golgi would affect 7a protein if the disassembly occurred before 7a protein triggered the inhibition of translation and activation of p38 MAPK. However, the Golgi appears to be fragmented at the end stages of apoptosis after the activation of caspases and just prior to cell death (14, 30). In cells expressing 7a protein, the Golgi appears intact at 24 h posttransfection (data not shown). Thus, expression of 7a protein appears to activate p38 MAPK, inhibit translation, and activate caspase-3 before the disassembly of the Golgi.

Very few Golgi proteins have been demonstrated to be pro- or antiapoptotic. One proapoptotic Golgi protein is protein kinase C theta (PKC θ), one of the isoforms of PKC (29). It is involved in the maturation, proliferation, and cytokine synthesis of T cells. The mechanism of apoptosis is unknown, but PKC θ activates the JNK MAPK pathway, and this activation may have a role in apoptosis (36). An antiapoptotic Golgi protein is baculovirus inhibitor of apoptosis repeat containing ubiquitin-conjugating enzyme (BRUCE) (7). BRUCE prevents apoptosis by antagonizing proapoptotic proteins such as caspase-3, caspase-9, and the second mitochondrial activator of caspases/direct IAP binding protein with low pI (designated smac/DIABLO) (26). BRUCE is essential for cell survival, since decreasing levels of BRUCE with RNA interference re-

sults in the induction of apoptosis (25, 27). One possibility is that expression of 7a protein leads to degradation and/or alteration of BRUCE, which results in the promotion of apoptosis. This hypothesis is currently under investigation.

To determine the role of 7a protein in the context of a viral infection, SARS-CoV viruses containing mutated or deleted 7a genes will have to be studied carefully. A SARS-CoV deletion virus that does not express 7a and 7b protein has been constructed and does not appear to induce apoptosis at a different rate from that of wild-type virus in tissue culture cells and mice (R. Baric et al., unpublished data). This would suggest that there are redundant proapoptotic proteins expressed by SARS-CoV. Indeed, it has recently been reported that 3a protein also induces apoptosis (15), and we have also observed that 7b and 9b induce apoptosis in tissue culture cells (unpublished data). However, it is probable that 7a protein does perform a function in disease progression in infected animals. Animal models that display disease symptoms similar to humans after infection with SARS-CoV, such as a ferret model, will be analyzed with wild-type and mutant viruses in the future.

It has not been determined whether infection with SARS-CoV causes an inhibition of cellular protein synthesis, but a potent inhibition of cellular protein synthesis is a characteristic feature of infection with another coronavirus, mouse hepatitis virus (9). It is not known whether just one viral protein is responsible for the inhibition of cellular protein synthesis in cells infected with mouse hepatitis virus, and it is plausible that SARS-CoV encodes additional proteins that inhibit cellular translation. The 7a protein may interact with a protein not involved directly in translation and may start an enzyme cascade, resulting in the inhibition of translation. The precise mechanism of cytopathogenesis of 7a protein is yet to be determined. However, the data presented here suggest that the SARS-CoV 7a protein inhibits translation and activates p38 MAPK.

ACKNOWLEDGMENTS

We thank Domenico Tortorella for the PDI antibody and Ralph Baric for the 7a antisera.

This work was partially supported by grants from the NIH (P.P.). Microscopy was performed at the MSSM-Microscopy Shared Resource Facility, supported in part with funding from an NIH-NCI shared resources grant (R24 CA095823). P.P. is a senior scholar of the Ellison Medical Foundation. S.A.K.-B. was partially supported by NIH training grant T32 A1007645.

REFERENCES

1. **Banerjee, S., K. Narayanan, T. Mizutani, and S. Makino.** 2002. Murine coronavirus replication-induced p38 mitogen-activated protein kinase activation promotes interleukin-6 production and virus replication in cultured cells. J. Virol. **76:**5937–5948.
2. **Barr, F. A., M. Puype, J. Vandekerckhove, and G. Warren.** 1997. GRASP65, a protein involved in the stacking of Golgi cisternae. Cell **91:**253–262.
3. **Chen, Y. Y., B. Shuang, Y. X. Tan, M. J. Meng, P. Han, X. N. Mo, Q. S. Song, X. Y. Qiu, X. Luo, Q. N. Gan, X. Zhang, Y. Zheng, S. A. Liu, X. N. Wang, N. S. Zhong, and D. L. Ma.** 2005. The protein X4 of severe acute respiratory syndrome-associated coronavirus is expressed on both virus-infected cells and lung tissue of severe acute respiratory syndrome patients and inhibits growth of Balb/c 3T3 cell line. Chin. Med. J. **118:**267–274.
4. **Ding, Y., L. He, Q. Zhang, Z. Huang, X. Che, J. Hou, H. Wang, H. Shen, L. Qiu, Z. Li, J. Geng, J. Cai, H. Han, X. Li, W. Kang, D. Weng, P. Liang, and S. Jiang.** 2004. Organ distribution of severe acute respiratory syndrome (SARS) associated coronavirus (SARS-CoV) in SARS patients: implications for pathogenesis and virus transmission pathways. J. Pathol. **203:**622–630.
5. **Donoghue, M., F. Hsieh, E. Baronas, K. Godbout, M. Gosselin, N. Stagliano, M. Donovan, B. Woolf, K. Robison, R. Jeyaseelan, R. E. Breitbart, and S. Acton.** 2000. A novel angiotensin-converting enzyme-related carboxypeptidase (ACE2) converts angiotensin I to angiotensin 1–9. Circ. Res. **87:**E1–E9.
6. **Fielding, B. C., Y. J. Tan, S. Shuo, T. H. Tan, E. E. Ooi, S. G. Lim, W. Hong, and P. Y. Goh.** 2004. Characterization of a unique group-specific protein (U122) of the severe acute respiratory syndrome coronavirus. J. Virol. **78:** 7311–7318.
7. **Hauser, H. P., M. Bardroff, G. Pyrowolakis, and S. Jentsch.** 1998. A giant ubiquitin-conjugating enzyme related to IAP apoptosis inhibitors. J. Cell Biol. **141:**1415–1422.
8. **Hicks, S. W., and C. E. Machamer.** 2002. The NH2-terminal domain of Golgin-160 contains both Golgi and nuclear targeting information. J. Biol. Chem. **277:**35833–35839.
9. **Hilton, A., L. Mizzen, G. MacIntyre, S. Cheley, and R. Anderson.** 1986. Translational control in murine hepatitis virus infection. J. Gen. Virol. **67:** 923–932.
10. **Itani, O. A., K. L. Cornish, K. Z. Liu, and C. P. Thomas.** 2003. Cycloheximide increases glucocorticoid-stimulated alpha-ENaC mRNA in collecting duct cells by p38 MAPK-dependent pathway. Am. J. Physiol. Renal Physiol. **284:**F778–F787.
11. **Kim, Y. H., M. R. Choi, D. K. Song, S. O. Huh, C. G. Jang, and H. W. Suh.** 2000. Regulation of c-fos gene expression by lipopolysaccharide and cycloheximide in C6 rat glioma cells. Brain Res. **872:**227–230.
12. **Kopecky, S. A., and D. S. Lyles.** 2003. Contrasting effects of matrix protein on apoptosis in HeLa and BHK cells infected with vesicular stomatitis virus are due to inhibition of host gene expression. J. Virol. **77:**4658–4669.
13. **Kopecky, S. A., and D. S. Lyles.** 2003. The cell-rounding activity of the vesicular stomatitis virus matrix protein is due to the induction of cell death. J. Virol. **77:**5524–5528.
14. **Lane, J. D., J. Lucocq, J. Pryde, F. A. Barr, P. G. Woodman, V. J. Allan, and M. Lowe.** 2002. Caspase-mediated cleavage of the stacking protein GRASP65 is required for Golgi fragmentation during apoptosis. J. Cell Biol. **156:**495–509.
15. **Law, P. T., C. H. Wong, T. C. Au, C. P. Chuck, S. K. Kong, P. K. Chan, K. F. To, A. W. Lo, J. Y. Chan, Y. K. Suen, H. Y. Chan, K. P. Fung, M. M. Waye, J. J. Sung, Y. M. Lo, and S. K. Tsui.** 2005. The 3a protein of severe acute respiratory syndrome-associated coronavirus induces apoptosis in Vero E6 cells. J. Gen. Virol. **86:**1921–1930.
16. **Li, J., and N. J. Holbrook.** 2004. Elevated gadd153/chop expression and enhanced c-Jun N-terminal protein kinase activation sensitizes aged cells to ER stress. Exp. Gerontol. **39:**735–744.
17. **Li, T., Z. Qiu, Y. Han, Z. Wang, H. Fan, W. Lu, J. Xie, X. Ma, and A. Wang.** 2003. Rapid loss of both CD4+ and CD8+ T lymphocyte subsets during the acute phase of severe acute respiratory syndrome. Chin. Med. J. **116:**985–987.
18. **Li, T., Z. Qiu, L. Zhang, Y. Han, W. He, Z. Liu, X. Ma, H. Fan, W. Lu, J. Xie, H. Wang, G. Deng, and A. Wang.** 2004. Significant changes of peripheral T lymphocyte subsets in patients with severe acute respiratory syndrome. J. Infect. Dis. **189:**648–651.
19. **Li, W., M. J. Moore, N. Vasilieva, J. Sui, S. K. Wong, M. A. Berne, M. Somasundaran, J. L. Sullivan, K. Luzuriaga, T. C. Greenough, H. Choe, and M. Farzan.** 2003. Angiotensin-converting enzyme 2 is a functional receptor for the SARS coronavirus. Nature **426:**450–454.
20. **Mancini, M., C. E. Machamer, S. Roy, D. W. Nicholson, N. A. Thornberry, L. A. Casciola-Rosen, and A. Rosen.** 2000. Caspase-2 is localized at the Golgi complex and cleaves golgin-160 during apoptosis. J. Cell Biol. **149:**603–612.
21. **Marra, M. A., S. J. Jones, C. R. Astell, R. A. Holt, A. Brooks-Wilson, Y. S. Butterfield, J. Khattra, J. K. Asano, S. A. Barber, S. Y. Chan, A. Cloutier, S. M. Coughlin, D. Freeman, N. Girn, O. L. Griffith, S. R. Leach, M. Mayo, H. McDonald, S. B. Montgomery, P. K. Pandoh, A. S. Petrescu, A. G. Robertson, J. E. Schein, A. Siddiqui, D. E. Smailus, J. M. Stott, G. S. Yang, F. Plummer, A. Andonov, H. Artsob, N. Bastien, K. Bernard, T. F. Booth, D. Bowness, M. Czub, M. Drebot, L. Fernando, R. Flick, M. Garbutt, M. Gray, A. Grolla, S. Jones, H. Feldmann, A. Meyers, A. Kabani, Y. Li, S. Normand, U. Stroher, G. A. Tipples, S. Tyler, R. Vogrig, D. Ward, B. Watson, R. C. Brunham, M. Krajden, M. Petric, D. M. Skowronski, C. Upton, and R. L. Roper.** 2003. The genome sequence of the SARS-associated coronavirus. Science **300:**1399–1404.
22. **Mizutani, T., S. Fukushi, M. Saijo, I. Kurane, and S. Morikawa.** 2004. Phosphorylation of p38 MAPK and its downstream targets in SARS coronavirus-infected cells. Biochem. Biophys. Res. Commun. **319:**1228–1234.
23. **Nelson, C. A., A. Pekosz, C. A. Lee, M. S. Diamond, and D. H. Fremont.** 2005. Structure and intracellular targeting of the SARS-coronavirus Orf7a accessory protein. Structure (Cambridge) **13:**75–85.
24. **O'Donnell, R., R. C. Tasker, and M. F. Roe.** 2003. SARS: understanding the coronavirus. Apoptosis may explain lymphopenia of SARS. BMJ **327:**620. (Letter.)
25. **Qiu, X. B., S. L. Markant, J. Yuan, and A. L. Goldberg.** 2004. Nrdp1-mediated degradation of the gigantic IAP, BRUCE, is a novel pathway for triggering apoptosis. EMBO J. **23:**800–810.
26. **Qiu, X. B., and A. L. Goldberg.** 2005. The membrane-associated inhibitor of

apoptosis protein, BRUCE/Apollon, antagonizes both the precursor and mature forms of Smac and caspase-9. J. Biol. Chem. **280:**174–182.
27. **Ren, J., M. Shi, R. Liu, Q. H. Yang, T. Johnson, W. C. Skarnes, and C. Du.** 2005. The Birc6 (Bruce) gene regulates p53 and the mitochondrial pathway of apoptosis and is essential for mouse embryonic development. Proc. Natl. Acad. Sci. USA **102:**565–570.
28. **Rota, P. A., M. S. Oberste, S. S. Monroe, W. A. Nix, R. Campagnoli, J. P. Icenogle, S. Penaranda, B. Bankamp, K. Maher, M. H. Chen, S. Tong, A. Tamin, L. Lowe, M. Frace, J. L. DeRisi, Q. Chen, D. Wang, D. D. Erdman, T. C. Peret, C. Burns, T. G. Ksiazek, P. E. Rollin, A. Sanchez, S. Liffick, B. Holloway, J. Limor, K. McCaustland, M. Olsen-Rasmussen, R. Fouchier, S. Gunther, A. D. Osterhaus, C. Drosten, M. A. Pallansch, L. J. Anderson, and W. J. Bellini.** 2003. Characterization of a novel coronavirus associated with severe acute respiratory syndrome. Science **300:**1394–1399.
29. **Schultz, A., J. I. Jonsson, and C. Larsson.** 2003. The regulatory domain of protein kinase Cθ localises to the Golgi complex and induces apoptosis in neuroblastoma and Jurkat cells. Cell Death Differ. **10:**662–675.
30. **Sesso, A., D. T. Fujiwara, M. Jaeger, R. Jaeger, T. C. Li, M. M. Monteiro, H. Correa, M. A. Ferreira, R. I. Schumacher, J. Belisario, B. Kachar, and E. J. Chen.** 1999. Structural elements common to mitosis and apoptosis. Tissue Cell **31:**357–371.
31. **Shorter, J., M. B. Beard, J. Seemann, A. B. Dirac-Svejstrup, and G. Warren.** 2002. Sequential tethering of Golgins and catalysis of SNAREpin assembly by the vesicle-tethering protein p115. J. Cell Biol. **157:**45–62.
32. **Tan, Y. J., B. C. Fielding, P. Y. Goh, S. Shen, T. H. Tan, S. G. Lim, and W. Hong.** 2004. Overexpression of 7a, a protein specifically encoded by the severe acute respiratory syndrome coronavirus, induces apoptosis via a caspase-dependent pathway. J. Virol. **78:**14043–14047.
33. **Tan, Y. J., E. Teng, S. Shen, T. H. Tan, P. Y. Goh, B. C. Fielding, E. E. Ooi, H. C. Tan, S. G. Lim, and W. Hong.** 2004. A novel severe acute respiratory syndrome coronavirus protein, U274, is transported to the cell surface and undergoes endocytosis. J. Virol. **78:**6723–6734.
34. **Tipnis, S. R., N. M. Hooper, R. Hyde, E. Karran, G. Christie, and A. J. Turner.** 2000. A human homolog of angiotensin-converting enzyme. Cloning and functional expression as a captopril-insensitive carboxypeptidase. J. Biol. Chem. **275:**33238–33243.
35. **Wang, H., Y. Mao, L. Ju, J. Zhang, Z. Liu, X. Zhou, Q. Li, Y. Wang, S. Kim, and L. Zhang.** 2004. Detection and monitoring of SARS coronavirus in the plasma and peripheral blood lymphocytes of patients with severe acute respiratory syndrome. Clin. Chem. **50:**1237–1240.
36. **Werlen, G., E. Jacinto, Y. Xia, and M. Karin.** 1998. Calcineurin preferentially synergizes with PKC-theta to activate JNK and IL-2 promoter in T lymphocytes. EMBO J. **17:**3101–3111.
37. **Wong, R. S., A. Wu, K. F. To, N. Lee, C. W. Lam, C. K. Wong, P. K. Chan, M. H. Ng, L. M. Yu, D. S. Hui, J. S. Tam, G. Cheng, and J. J. Sung.** 2003. Haematological manifestations in patients with severe acute respiratory syndrome: retrospective analysis. BMJ **326:**1358–1362.
38. **Yan, H., G. Xiao, J. Zhang, Y. Hu, F. Yuan, D. K. Cole, C. Zheng, and G. F. Gao.** 2004. SARS coronavirus induces apoptosis in Vero E6 cells. J. Med. Virol. **73:**323–331.